We are IntechOpen,
the world's leading publisher of
Open Access books
Built by scientists, for scientists

4,800
Open access books available

122,000
International authors and editors

135M
Downloads

Our authors are among the

154
Countries delivered to

TOP 1%
most cited scientists

12.2%
Contributors from top 500 universities

BOOK CITATION INDEX
CLARIVATE ANALYTICS
INDEXED

WEB OF SCIENCE™

Selection of our books indexed in the Book Citation Index
in Web of Science™ Core Collection (BKCI)

Interested in publishing with us?
Contact book.department@intechopen.com

Numbers displayed above are based on latest data collected.
For more information visit www.intechopen.com

Analysis of Oxide on Steam Generator Tubing Material in High Temperature Alkaline Leaded Solution

Dong-Jin Kim, Seong Sik Hwang, Joung Soo Kim, Yun Soo Lim,
Sung Woo Kim and Hong Pyo Kim
Korea Atomic Energy Research Institute
1045 Daedeok-Daero, Yuseong-Gu, Daejeon 305-353
Republic of Korea

1. Introduction

Nuclear power plants (NPP) using Alloy 600 as a heat exchanger tube of the steam generator (SG) have experienced various corrosion problems such as pitting, intergranular attack (IGA) and stress corrosion cracking (SCC). In spite of much effort to reduce the material degradations, SCC is still one of important problems to overcome.

Secondary water pH which affects SCC behavior substantially spans widely from acid to alkaline in crevice depending on water chemistry control, water chemistry in crevice, plant specific condition, etc. Especially, specific chemical species are accumulated in the crevice as the sludge leading to a specific condition of crevice chemistry. Among these chemical species, lead is known to be one of the most deleterious species in the reactor coolants that cause SCC of the alloy (Sarver, 1987; Castano-Marin et al., 1993; Wright and Mirzai, 1999; Staehle, 2003). Even Alloy 690, as an alternative of Alloy 600 because of outstanding superiority to SCC, is also susceptible to lead in alkaline solution (Vaillant et al., 1996; Kim et al., 2005; Kim and Kim, 2009).

Lead has been effectively detected in all tubesheet samples, crevice deposits and surface scales removed from SGs. Typical concentrations are 100 to 500 ppm but in some plants, concentrations as high as 2,000 to 10,000 ppm have been detected (Fruzzetti, 2005). The best method to prevent lead induced SCC (PbSCC) is to eliminate the harmful lead from the NPP chemistry, which is not possible and most NPPs are already contaminated by lead. Moreover only a very low level of sub ppm affects PbSCC.

During a long exposure time of more than 30 years under a high temperature and high pressure water chemical environment, an Alloy 600 surface experiences an oxide formation, breakdown and modification depending on the nature of the grown oxide, combined with a residual stress induced by a tube expansion which is introduced to fix a tube to a tube sheet. Therefore it is strongly anticipated that a SCC is inevitably related to an oxide properties, formed on an Alloy 600 surface, because a crack initiates and propagates through a breakdown and alteration of a surface oxide, fundamentally speaking. An oxide properties should be investigated for the elucidation of a lead induced mechanism and its countermeasure.

It is expected that an addition of lead into a solution modifies the oxide property affecting SCC behavior. A discovery of the way to avoid this modification can give us a key to control PbSCC such as an inhibitor.

The thickness, composition, passivity and structure of an oxide formed and grown on Alloy 600 are influenced by the temperature, pH, time, chemical species and so on, in a very complex manner (McIntyre et al., 1979; Kim et al., 2008). The very complicated and nano-sized thin oxides formed in aqueous/non aqueous conditions have been successfully analysed by using a transmission electron microscopy (TEM), an x-ray photoelectron spectroscopy (XPS), an Auger electron spectroscopy (AES) and an electrochemical impedance spectroscopy (EIS) (Machet et al., 2004; Yi et al., 2005; Rincón et al., 2007; Hwang et al., 2007).

In the present work, the oxides formed on Alloy 600 in aqueous solutions with and without lead were examined by using a transmission electron microscopy (TEM), an energy dispersive x-ray spectroscopy (EDXS), an x-ray photoelectron spectroscopy (XPS) and an electrochemical impedance spectroscopy (EIS). The oxide property was compared with the SCC behaviors tested in caustic solutions in the presence of lead and NiB as an inhibitor as well as in the absence of both impurities by using a slow strain rate tension (SSRT) test.

2. Experimental details

The test specimens were fabricated from a 19.05 mm (0.75 inches) outside diameter Alloy 600 steam generator tubing material which was thermally treated (TT) at 704°C for 15 hours following solution annealing at 975°C for 20 minutes or high temperature mill annealed (HTMA) at 1024°C for 3 minutes. The chemical compositions are given in Table 1. High-purity water (18MΩ·cm at RT) was used as the reference solution. Aqueous solutions used were shown in Table 2. Reagent grade PbO was added to the reference solution at an amount of 5,000 or 10,000 ppm as a source of lead. The performance of a NiB inhibitor was evaluated by adding 4 g/l of NiB into the leaded solution. Deaeration was carried out by purging with a high purity nitrogen gas to remove the dissolved oxygen for 20 hours before the tests commenced.

Material	C	Si	Mn	P	Cr	Ni	Fe	Co	Ti	Cu	Al	B	S	N	Ce
Alloy 600TT	0.03	0.07	0.003	0.024	16.12	74.42	9.06	0.007	0.005	0.003		0.006	0.001	0.0103	0.003
Alloy 600 HTMA	0.025	0.05	0.22	0.07	15.67	75.21	8.24	0.005	0.39	0.011	0.15	0.0014	0.001	0.0103	

Table 1. Chemical compositions of the Alloy 600 TT and Alloy 600 HTMA

The electrochemical tests were performed for rectangular plate specimens (10 mm x 10 mm) fabricated from the thermally treated tubing. The surface of the specimens was polished up to 1 μm using a diamond suspension. An Alloy 600 wire was spot welded to the specimen, and the wire was shielded with a heat-shrinkable polytetrafluoroethylene (PTFE) tubing. The test specimens were immersed in a 1-gallon nickel autoclave at 315°C for 14 days. The electrochemical impedance measurements were carried out in the frequency range of 10^6 to 10^{-3} Hz at the OCP with a 10 mV perturbation. A Solartron 1255 frequency response analyser was used with a Solartron 1287 electrochemical interface. Experimental matrix was shown in

Table 2. Separate autoclaves were used for the leaded and the unleaded test solutions to avoid a cross contamination.

Environment	pH(315°C) by MULTEQ	Remark	Experiment
-H₂O	5.8	Neutral	
-10,000ppm PbO	7.9	pH increase	SSRT test
-10,000ppm PbO + 4g/L NiB	7.9	Deaeration	
-0.01M Na₂SO₄ + 0.01M NaHSO₄	5.6	Acid	
-10,000ppm PbO	8.7	pH increase	SSRT test
-10,000ppm PbO + 4g/L NiB	8.7	Deaeration	
-0.01M Na₂SO₄	5.8	Neutral	
-10,000ppm PbO	8.6	pH increase	SSRT test
-10,000ppm PbO + 4g/L NiB	8.6		
-Ammonia	6.3	Mild caustic	
-5,000ppm PbO	7.9	pH increase	Immersion test
-5,000ppm PbO + 4g/L NiB	7.9	Deaeration	
-0.1M NaOH (Deaeration)	9.9		
-5,000/10,000ppm PbO (Deaeration)	9.9	Caustic	SSRT, immersion test
-5,000/10,000ppm PbO (Non-deaeration)	9.9	the Same pH	
-10wt% NaOH	10.4	Strong caustic	
-10,000ppm PbO	10.4	Deaeration	SSRT test
-40wt% NaOH	10.9	Strong caustic	
-10,000ppm PbO	10.9	Deaeration	SSRT test

Table 2. Various aqueous solutions and their pHs for SSRT and immersion (electrochemical impedance) tests at 315°C (MULTEQ, 2008)

After the immersion test, the plate specimens were examined. The surface oxide layer and its composition was examined by using a field emission TEM, equipped with an EDXS (JEM-2100F, JEOL). The information on the chemical binding was obtained by using an XPS (AXIS-NOVA, KRATOS Analytical) The spectra for Ni 2p, Cr 2p, O 1s and Pb 4f were recorded with an AlKα radiation (hν = 1486.6 eV), at a pass energy of 20 eV. The take-off angle, the base pressure and the sputter rate for a depth profiling were 45°, 5.0×10^{-9} torr and 0.04nm/s in SiO_2, respectively. To analyse the XPS results, an online database was used (http://www.laserface.com).

The SSRT tests were performed for uniaxial tension specimens fabricated from a HTMA tubing in unleaded, and leaded solutions, and a leaded one with a NiB addition. The tests were carried out in 0.5-gallon nickel autoclaves at 315˚C and an equilibrium pressure. The test specimens were at an open circuit potential (OCP) without an impressed electrochemical current. The strain rate was 2×10^{-7} s⁻¹. After the SSRT test, surface was observed to determine SCC ratio by using a SEM (JSM6360).

3. Results and discussion

3.1 Analysis of oxide in solution without lead

Figs. 1 (a) and (b) are the TEM images and the results of the TEM-EDXS analyses for a cross-section of the surface oxide layer that was formed in the ammonia solution without/with

NiB at 315°C, respectively. Similar appearance was observed for the two oxide layers formed in the two kinds of solutions with about a 400 – 500 nm thickness. An inner oxide layer can be more clearly differentiated in the surface oxide formed in the ammonia solution with NiB. It is worthwhile noting that an outer layer seems to be more porous compared to an inner layer.
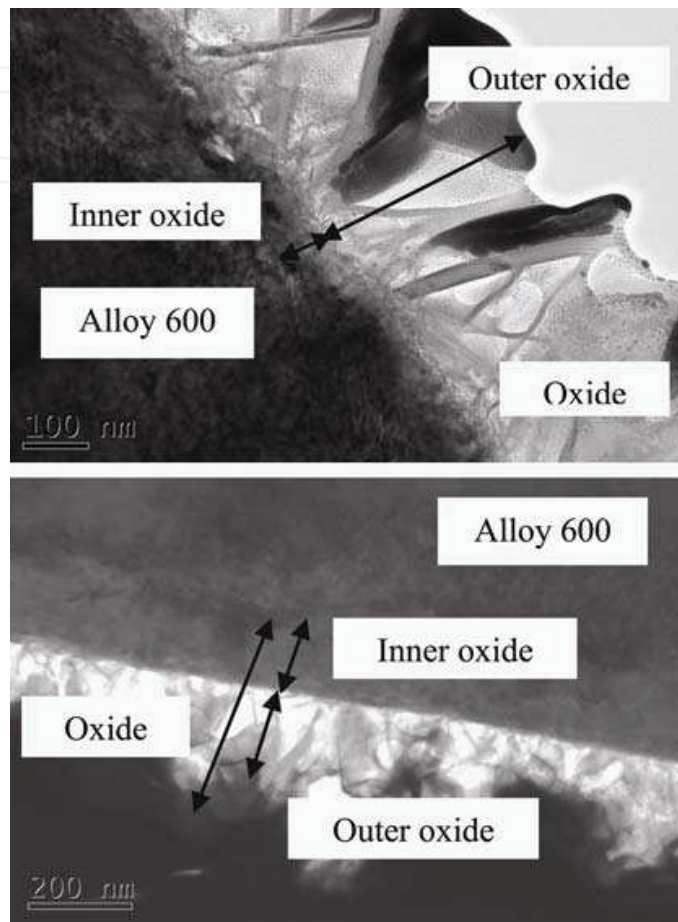
(a)

Fig. 1. (a) TEM images for surface oxides formed on Alloy 600 specimens

From Fig. 1(b) of the TEM-EDXS results, the surface oxide layers are composed of a duplex oxide layer, i.e., nickel rich outer layer and chromium rich inner layer, irrespective of the used aqueous solution. A chromium rich inner layer of the surface oxide formed in the ammonia solution with NiB is thicker than that of the surface oxide layer in the ammonia solution without NiB. Based on the similar chemical composition and surface appearance of both surface oxide layers, except for the oxide thickness, the TEM diffraction pattern for the surface oxide formed in the ammonia solution with NiB was analysed because it is easier to observe a thicker oxide.

Figs. 2 (a) and (b) are the diffraction patterns, mainly obtained from an outer surface oxide and an inner surface oxide, respectively. From the diffraction patterns, there are two ring patterns and two spot patterns. The same patterns corresponding to outer ring and spot pattern I are observed in Figs. 2 (a) and (b) because the beam size is too wide to differentiate a duplex layer, i.e. an outer surface oxide and an inner oxide, completely, even though the diffraction pattern was investigated at different sites. By analysing the diffraction pattern for

the surface oxide formed in the ammonia solution with NiB at 315°C, an outer ring and an inner ring originated from an inner oxide and an outer oxide, respectively. It was revealed that a porous outer oxide is mainly composed of NiO and a relatively dense inner layer consists of Cr_2O_3 (JCPDS card no. 47-1049; JCPDS card no. 74-0326). It seems that spot patterns I and II are related to another nickel oxide such as $Ni(OH)_2$ rather than NiO and Alloy 600, respectively.
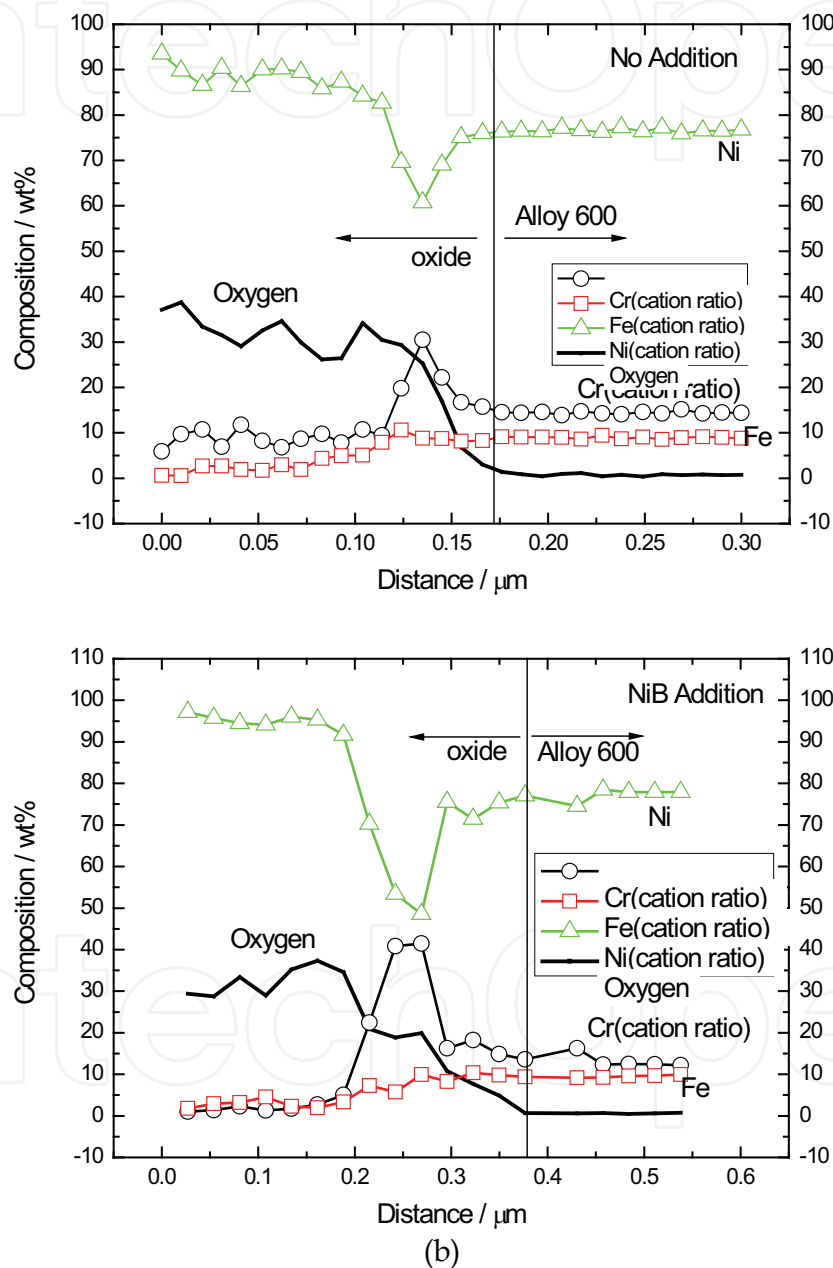

Fig. 1. (b) TEM-EDXS analyses for in-depth chemical compositions for surface oxide layer formed on Alloy 600 specimens in ammonia solutions without/with NiB at 315°C (Kim, D.-J. et al., 2010)

Figs. 3 (a) and (b) are the XPS results for the surface oxide formed in the ammonia solution with NiB. Ni metal with a binding energy in the range of 852.8~853 eV was detected near

the top surface oxide and its intensity increased rapidly to a saturation value with the etching time while the intensities for NiO and Ni(OH)$_2$ with binding energies near 855 eV and 856.6 eV, respectively, were very small even at a 10s etching time and their values were decreased to a background level only at a 1430s etching time. From the results of the diffraction pattern and XPS, it was found that an outer oxide is composed of NiO and Ni(OH)$_2$.
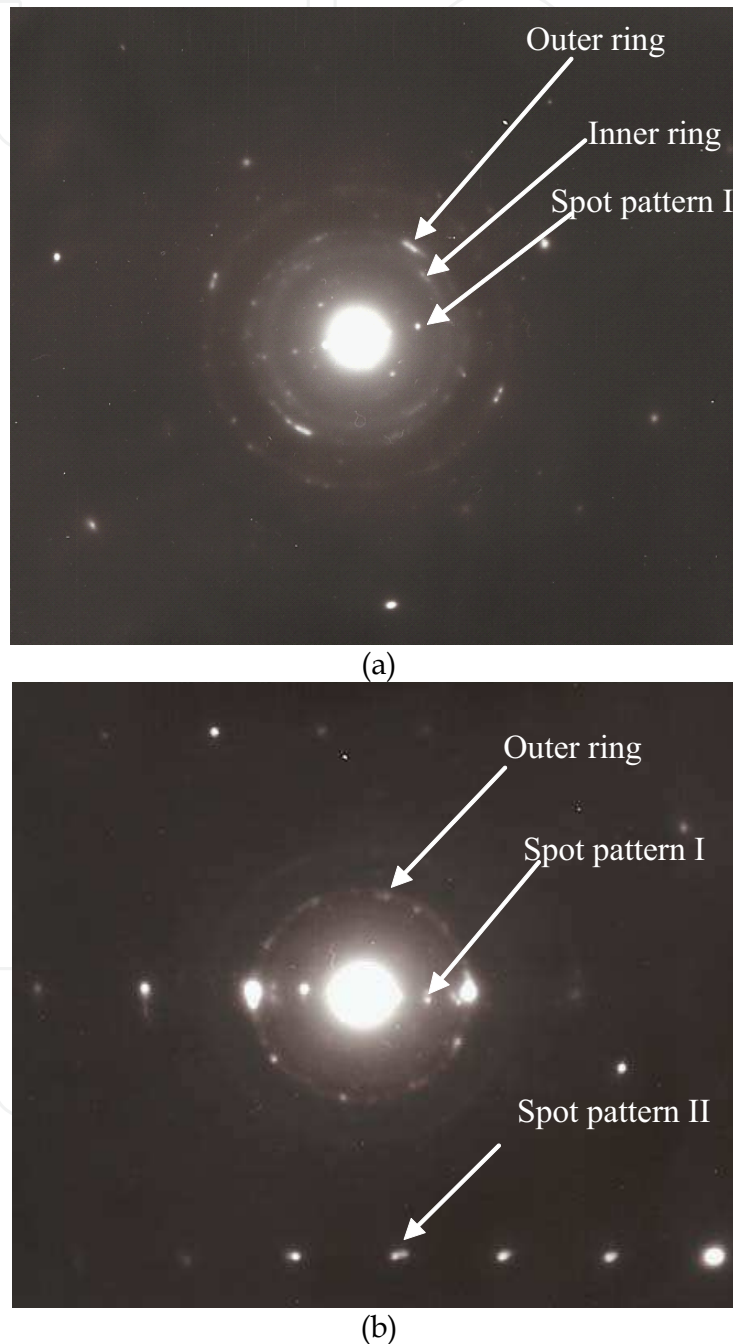

(a)

(b)

Fig. 2. Diffraction patterns for (a) outer surface oxide and (b) inner surface oxide formed on Alloy 600 in an ammonia solution with NiB at 315°C (Kim, D.-J. et al., 2010)

Apart from Ni, Cr metal with a binding energy of 574.2 eV did not appear at an early stage and the intensity of the metallic chromium increased with the sputtering time while the

intensity for the Cr oxide with a binding energy in the range of 576.6 to 577.3 eV revealed a large value at an early stage and decreased slowly with the etching time indicating that the Cr oxide is relatively dense.

Combining the results of the TEM and XPS, it can be concluded that the nickel oxides of NiO and Ni(OH)$_2$ are very porous and hence a porous outer oxide is sputtered easily leading to an early appearance of unreacted nickel while Cr oxide composed of an inner layer is much denser than an outer layer. It has been reported that metallic ions in a solution are re-deposited to form a porous outer oxide layer (Robertson, 1989). Growth processes of an inner layer and an outer layer occur at the metal/oxide and oxide/electrolyte interfaces, respectively. The growth rates are controlled by a transport of the layer forming species through a layer, i.e. by an inward diffusion of electrolyte species including oxygen and an outward diffusion of metal cations.


(a)

(b)
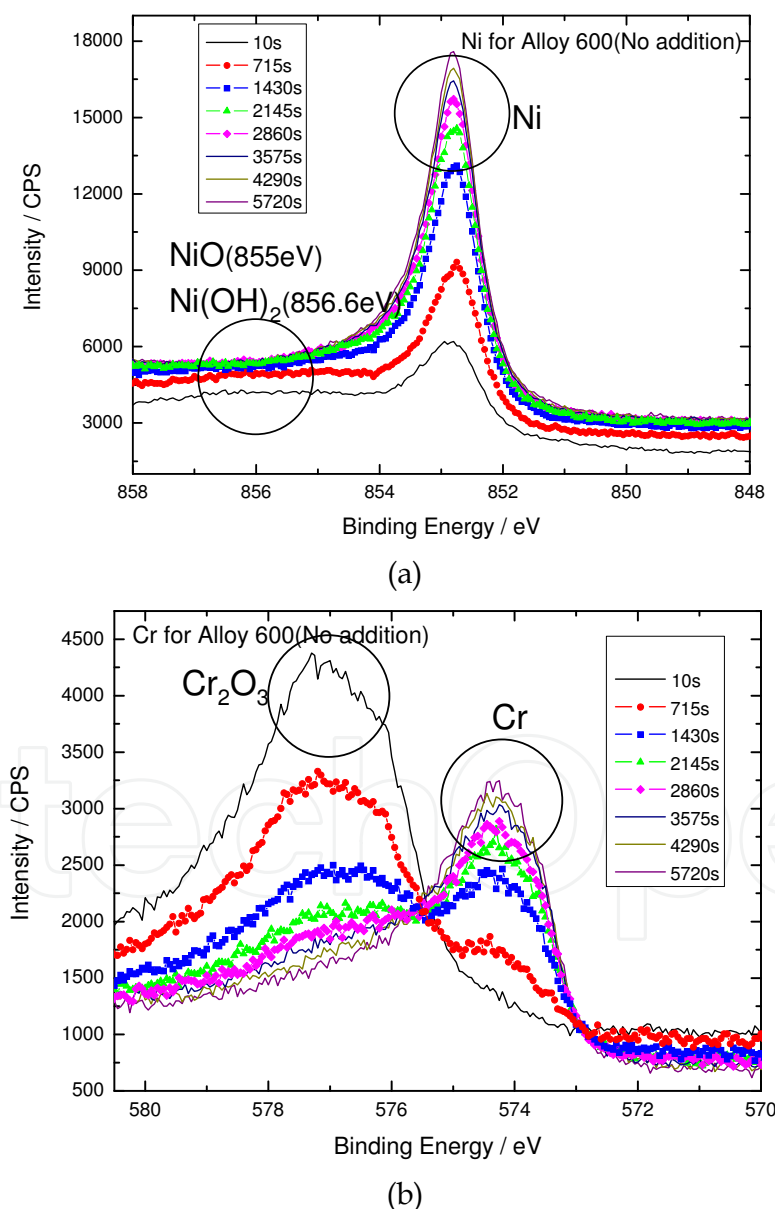
Fig. 3. X-ray photoelectron spectra of (a) Ni(2p3/2) and (b) Cr(2p3/2) for surface oxide layer formed in an ammonia solution without additive at 315°C (Kim, D.-J. et al., 2010)

3.2 Analysis of oxide in solution with lead

Fig. 4 is TEM micrographs for the surface oxide layer formed on the TT Alloy 600 specimens in aqueous solutions at 315°C of (a) unleaded 0.1M NaOH (reference) and (b) with PbO. In the unleaded solution, porous outer oxide and inner oxide are observed while only an oxide layer is observed in the leaded solution.
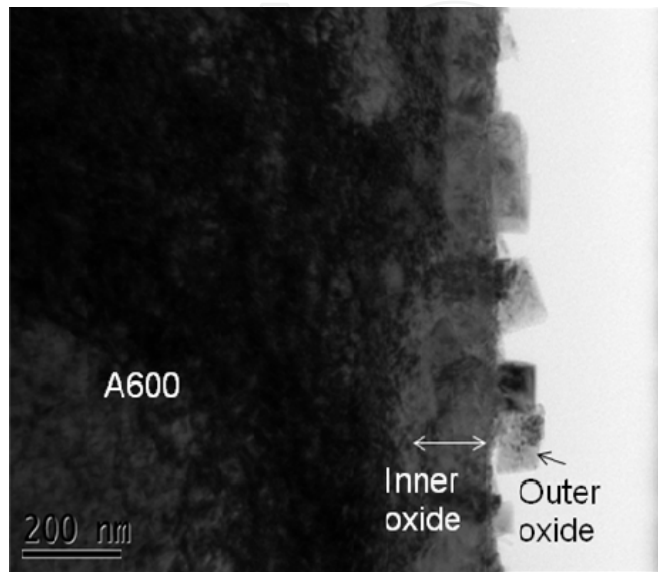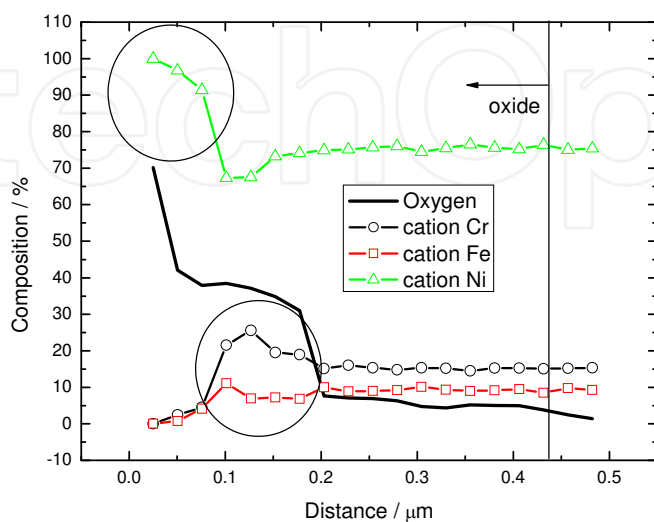

(a)
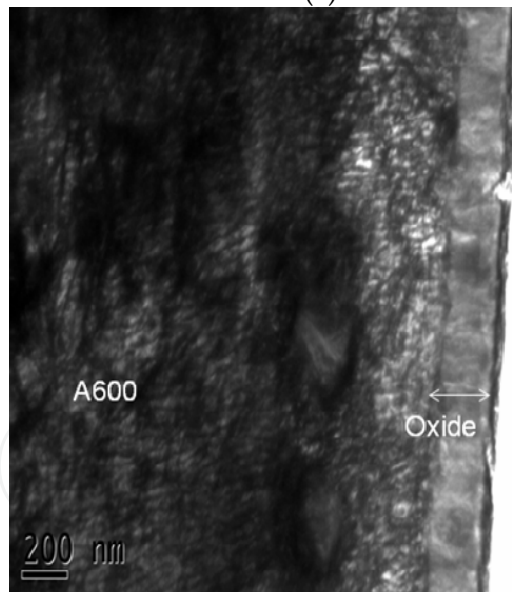
(b)

Fig. 4. TEM micrographs for the surface oxide layer formed on the TT Alloy 600 specimens in aqueous solutions at 315°C; (a) unleaded 0.1M NaOH (reference) and (b) with PbO
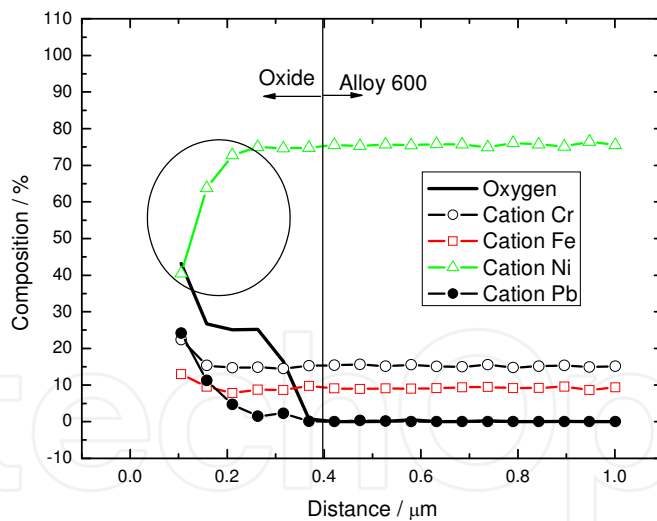
Fig. 5 shows the TEM-EDXS analyses for the specimens tested in the unleaded reference 0.1M NaOH solution (Fig. 5a) and in the leaded solution (Fig. 5b). From the results of Figs. 4 and 5, a duplex oxide layer was formed at the surface, i.e., porous nickel-rich outer layer and dense chromium-rich inner layer similar to the experimental results obtained in unleaded ammonia solution. In the leaded solution, a large amount of lead was observed at about 25

% on the surface. Cations such as Cr and especially Ni were depleted in the oxide layer. The duplex oxide layer observed in the unleaded solution was not examined in the leaded solution.


(a)

(b)

Fig. 5. TEM-EDXS analyses for the in-depth chemical compositions for the surface oxide layer formed on the TT Alloy 600 specimens in aqueous solutions at 315°C; (a) unleaded 0.1M NaOH (reference) and (b) with PbO

It is interesting to see the electrochemical impedance spectroscopy (EIS) results obtained for the specimens immersed in the aqueous solutions without/with PbO. Fig. 6 presents the Nyquist plots obtained for the TT Alloy 600 specimens in the 0.1 M NaOH solutions at 315°C of (a) the unleaded reference and (b) the leaded solution. From the impedance spectra

obtained for the unleaded solution, it can be assumed that the equivalent circuit is composed of a series of a solution resistance and a parallel of a capacitance and a resistance originating from a passive oxide and a constant phase element which may be related to a diffusion process of an electrolyte or a metallic cation, connected to an oxide resistance.
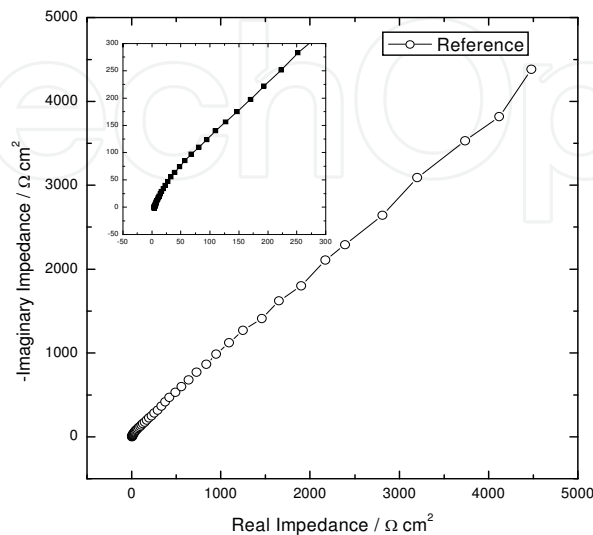
(a)
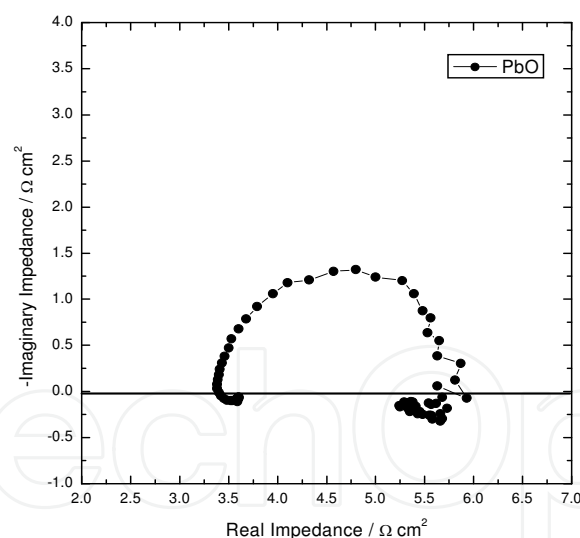
(b)

Fig. 6. Nyquist plots obtained from the electrochemical impedance measurements for the TT Alloy 600 immersed in the 0.1 M NaOH solutions at 315°C: (a) unleaded reference and (b) leaded with PbO

However, by adding lead oxide to the solution, the total impedance was considerably decreased indicating that an oxide passivity was greatly decreased. An inductive loop which might be caused by a lead incorporation into the oxide was observed. This inductive loop may be attributed to conduction path by the incorporated lead.

Fig. 7 shows the XPS results for the specimen tested in the leaded ammonia solution. Lead is incorporated into the oxide layer at a metallic state (136.7 eV) and as a lead oxide (138.9 eV) (http://www.lasurface.com).

Based on thermodynamics, an equilibrium electrochemical potential of Pb^{2+}/Pb is higher than an equilibrium potential of Ni^{2+}/Ni leading to increase of OCP of Alloy 600 in the leaded solution (Pourbaix, 1966). Hence, Pb can be deposited electrochemically in the leaded solution at OCP, which is consistent to Pb metal detected by XPS. However it is not unequivocal yet which one between metallic Pb and PbO affects PbSCC more.
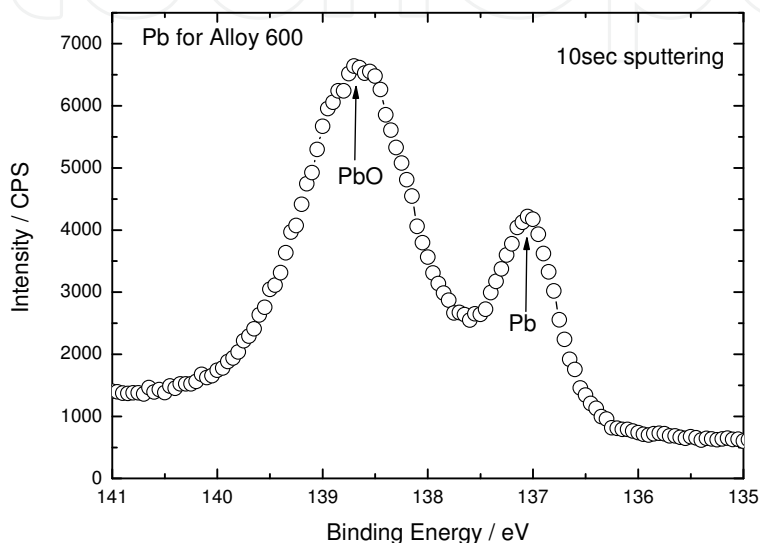

Fig. 7. X-ray photoelectron spectrum of the surface oxide layer formed for TT Alloy 600 in the leaded ammonia solution
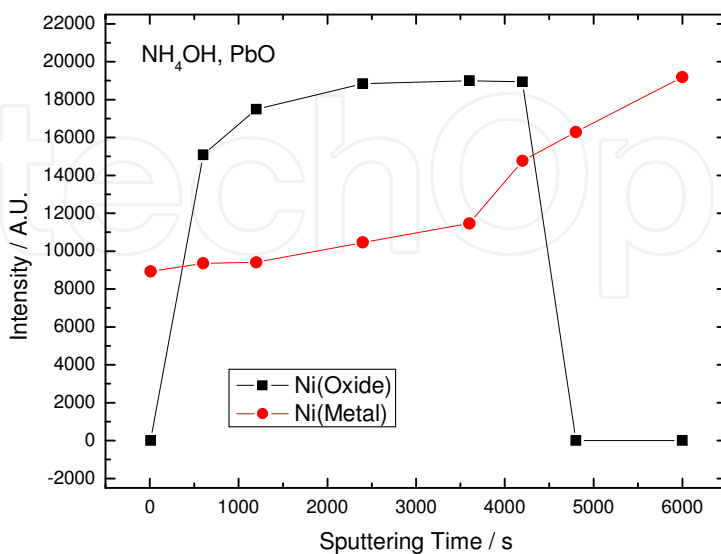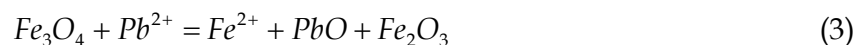

Fig. 8. Plot of XPS intensity of nickel as a metallic state and metal as an oxide state against sputtering time obtained for a TT Alloy 600 specimen immersed in leaded ammonia solution

Fig. 8 is a plot of the XPS intensity of Ni as a metallic state and Ni as an oxide state against sputtering time obtained for a specimen immersed in leaded ammonia solution. Fig. 8 was obtained by integration the XPS signal acquired around binding energy level of the Ni species as a metallic state and an oxide state as a function of the sputtering time. Depletion of nickel as an oxide state and a metallic state was observed in the oxide formed in an ammonia solution including PbO, which is consistent with Ni depletion in the oxide shown in Figs. 1 and 5.

In order to investigate reactions available during the experiment, eight reactions were considered as follows.

$$NiO + Pb^{2+} = PbO + Ni^{2+} \tag{1}$$

$$Cr_2O_3 + 3Pb^{2+} = 3PbO + 2Cr^{3+} \tag{2}$$

$$Fe_3O_4 + Pb^{2+} = Fe^{2+} + PbO + Fe_2O_3 \tag{3}$$

$$Ni^{2+} + Pb = Ni + Pb^{2+} \tag{4}$$

$$2Cr^{3+} + 3Pb = 2Cr + 3Pb^{2+} \tag{5}$$

$$Fe^{2+} + Pb = Fe + Pb^{2+} \tag{6}$$

$$Pb^{2+} + H_2O = PbO + 2H^+ \tag{7}$$

$$Pb + H_2O = PbO + H_2 \tag{8}$$

Based on thermodynamic data and solubility (MULTEQ, 2008; HSC chemistry database), forward reaction is available for reaction (1) at 315ºC assuming that concentrations of nickel and lead ions are 10^{-6} mole and 0.0045 mole, respectively. This reaction can be rewritten as follows by using defect chemistry.

$$Ni_{Ni} = Ni^{2+} + V_{Ni}^{2-} \tag{9}$$

$$V_{Ni}^{2-} + Pb^{2+} = Pb_{Ni} \tag{10}$$

By summing reactions (9) and (10), reaction (11) expressing that Ni at Ni site in the oxide is dissolved leaving Ni vacancy and lead ion reacts with Ni vacancy to be oxidized is obtained.

$$Ni_{Ni} + Pb^{2+} = Ni^{2+} + Pb_{Ni} \tag{11}$$

From reaction (11), Ni as a Ni oxide state can be depleted as shown in Fig. 9 and a strain field in the oxide originating from lattice mismatch can be also generated leading to a degradation of passivity.

However, the backward reaction of reactions (2) and (3) is available indicating that a substitution of lead ion for cations such as Cr and Fe in the oxide is not possible at 315ºC. Backward reactions for reactions (4)~(6) describing lead electrodeposition are available. From this, cations in the oxide formed in the leaded aqueous solution can be depleted by lead electrodeposition and moreover, the electrodeposited lead can prevent a formation of

the passive oxide composed of Ni, Cr, Fe and O, especially passive chromium oxide which is formed in the aqueous solution without Pb.

Considering thermodynamics for reactions (7) and (8), lead ion in an aqueous solution and electrodeposited lead are oxidized when a pH at 315oC is larger than 4.46 and a hydrogen partial pressure is as low as the secondary water of NPP, respectively.

3.3 Stress corrosion cracking behavior

As shown in Table 2, pH at 315oC increases by adding PbO, which seems to be caused by $PbO + H_2O = Pb^{2+} + 2OH^-$ reaction (Pourbaix, 1966).

Table 3 shows the elongation to rupture and the SCC ratio as a function of the aqueous solution without/with PbO for HTMA Alloy 600. Elongation to rupture and SCC ratio were found from the stress-strain curve and fracture surface observation. Elongation to rupture and SCC ratio can be used as criteria for SCC susceptibility from the fact that yield strength and tensile strength are decreased with the stress corrosion cracking leading to the lower elongation to rupture. The SCC susceptibility was greatly increased up to 0.1M NaOH by adding PbO into the solution. PbO degraded SCC resistance in 10wt% NaOH (2.5M NaOH) where Alloy 600 showed SCC behavior without PbO. However the effect of PbO on SCC in 40wt% NaOH (10M NaOH) was less than that in 0.1M NaOH. Considering that a neutral pH at 315oC is 5.8, HTMA Alloy 600 is susceptible to a PbSCC in a mild caustic solution rather than a strong caustic solution such as 2.5M and 10M NaOH solutions. From the results of 10wt% and 40wt% NaOH solutions, there seems to be a pH range susceptible to PbSCC, which may be closely related to oxide stability such as Ni, Cr, Fe and Pb oxides in a strong caustic solution.

Environment	Elongation to rupture(%)	SCC ratio	pH(315oC) by MULTEQ	Remark
-H$_2$O	56	Little	5.8	Neutral
-10,000ppm PbO	30	83	7.9	pH increase
-0.01M Na$_2$SO$_4$ + 0.01M NaHSO$_4$	64	16	5.5	Acid
-10,000ppm PbO	40	57	8.7	pH increase
-0.01M Na$_2$SO$_4$	49	Little	7.5	Mild caustic
-10,000ppm PbO	26	81	8.6	pH increase
-0.1M NaOH (Deaeration)	57	Little	9.9	Caustic Susceptible to PbSCC
-10,000ppm PbO (Deaeration)	24	78	9.9	
-10,000ppm PbO (Non-deaeration)	35	48	9.9	
-10wt% NaOH (Deaeration)	55	17	10.4	Strong caustic
-10,000ppm PbO (Deaeration)	38	31	10.4	Susceptible to PbSCC
-40wt% NaOH (Deaeration)	61	Little	10.9	Strong caustic Relatively less susceptible
-10,000ppm PbO (Deaeration)	63	5	10.9	

Table 3. Elongation to rupture and SCC ratio obtained from SSRT test in various aqueous solutions at 315oC

Alloy 690 which consists of 60% Ni, 30% Cr and 10% Fe is not susceptible to stress corrosion cracking in mild caustic solution such as 0.1M NaOH with or without lead while Alloy 690 is very sensitive to stress corrosion cracking in highly caustic solution such as 2.5M NaOH solution, which is more aggravated with Pb (Kim and Kim, 2009). From this it was found that Alloy 690 is not immune to SCC but relatively stronger than Alloy 600.

HTMA Alloy 600 was more susceptible to PbSCC in deaerated solution rather than non-deaerated 0.1M NaOH solution. Pb electrodeposition is not available in non-deaearated solution while Pb is electrodeposited spontaneously in deaerated solution. This indicates that Pb electrodeposition is more important to PbSCC rather than PbO itself. It was also reported that lead ion can be incorporated by occupying a cation site in an oxide producing a metallic dissolution, which could introduce a lattice mismatch leading to a passivity degradation of the oxide and lead could be incorporated into the film as an oxide itself causing the passivity degradation by using the current transient experiment (Kim et al., 2010).
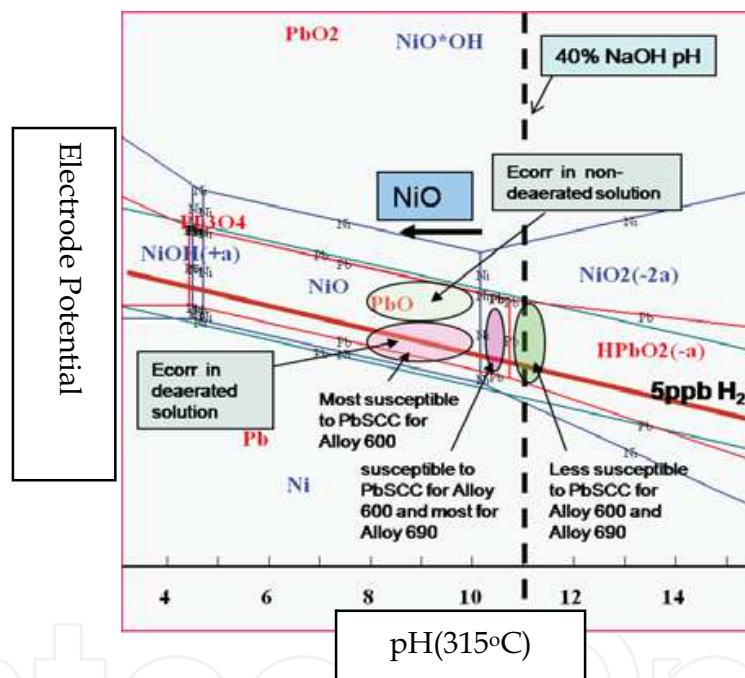

Fig. 9. E-pH diagram at 315°C

From the SSRT and EIS results, it was found that a better passivity improves the SCC resistance. In general, a repassivation of a more passive oxide is faster than that of a less passive oxide in the passive range leading to an SCC resistance. Moreover cracks initiate and propagate through unavoidable breakdowns and alterations of a surface oxide formed naturally on Alloy 600 in an aqueous solution indicating that a passivity is closely related to SCC resistance. Besides passivity, it was reported that the oxide ductility was degraded by lead incorporation into the solution (Lu et al., 2008).

It is notable that Ni among metallic elements which is a major element consisting of Alloy 600 was mainly depleted as shown in Figs. 1 and 5. For this reason, the kinetics of reactions should be considered. Generally, according to the E-pH diagram at a high temperature (HSC chemistry database), the lead contaminants could be reduced and deposited on an

oxide surface as a metallic form, or incorporated into the passive layer as lead ions or a lead oxide, depending on the OCP by the presence of a lead contamination in the secondary-side cooling water of operating NPP.

E-pH diagram at 315°C was shown in Fig. 9. Stable phases of Ni and Pb are also seen. SCC susceptible region for Alloy 600 and Alloy 690 was indicated in the figure.

3.4 PbSCC inhibitor

Fig. 10 presents the elongation to rupture as a function of the high temperature pH of leaded solutions without/with NiB for HTMA Alloy 600. An addition of NiB into the solution obviously enhances elongation to rupture.
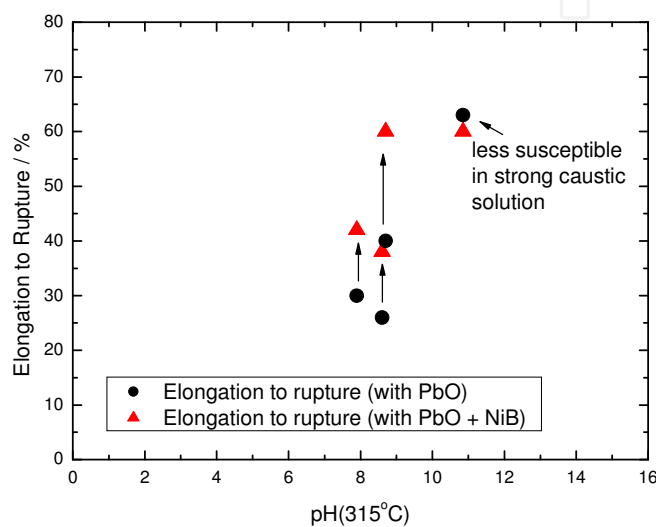
Fig. 10. Elongation to rupture as a function of the pH of leaded solutions without/with NiB for HTMA Alloy 600 (Kim, D.-J. et al., 2010)
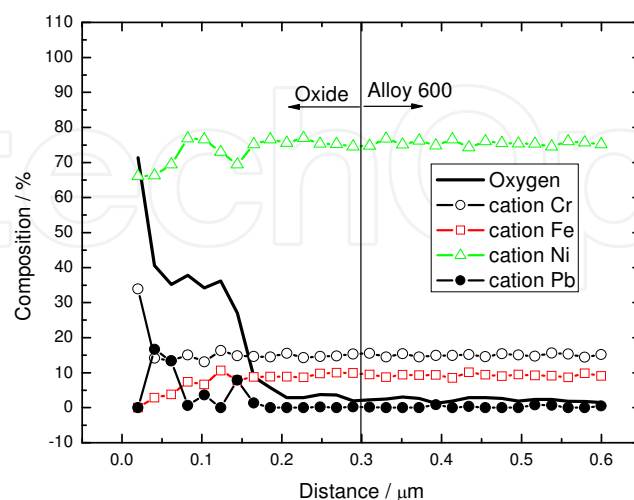

Fig. 11. TEM-EDXS analysis for the in-depth chemical compositions for the surface oxide layer formed on the TT Alloy 600 specimen in leaded 0.1M NaOH solution with NiB at 315°C

Fig. 12 is the XPS results for the specimens tested in the ammonia solution in the presence of PbO and PbO + NiB. Fig. 12 (a) reveals that the lead is incorporated into the oxide layer as a metallic state (136.7 eV) and as a lead oxide (138.9 eV). The lead content in the oxide was significantly decreased by adding NiB to the solution. Fig. 12 (b) is a plot of the XPS intensity against the sputtering time for the metallic lead and lead oxide. The amount of incorporated lead in the oxide was significantly decreased with the sputtering time. It was also found that the amount of incorporated lead was smaller and the lead inclusive layer was thinner in the specimen tested in the solution with NiB. Less incorporation of lead in the oxide led the enhancement of SCC resistance.

In the leaded solution with the NiB inhibitor, the amount of lead in the oxide layer was significantly reduced and the extent of the Ni depletion in the oxide was also decreased as shown in Fig. 11, compared with the results of Fig. 5.
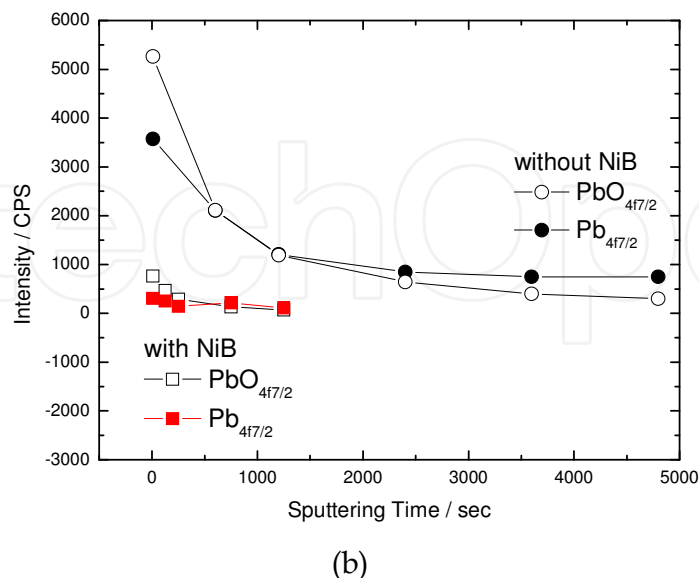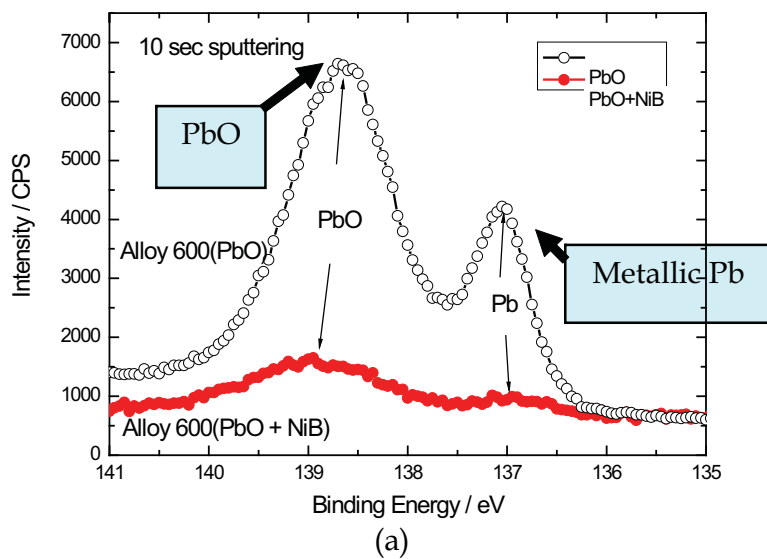

(a)

(b)

Fig. 12. (a) X-ray photoelectron spectra for surface oxide layer formed in leaded solution without/with NiB inhibitor at 315ºC and (b) intensity versus sputter time for PbO (4f7/2) and Pb (4f7/2) (Kim, D.-J. et al., 2010)

It is worthwhile to note that an impedance value obtained in the leaded solution with the NiB as shown in Fig. 13 significantly increased, compared with the impedance value obtained in the absence of NiB (Fig. 6). The impedance spectrum showed a clear capacitive arc but the inductive loop which appeared in the leaded solution did not appear. The impedance spectrum resembled the spectrum for the reference solution rather than that for the leaded solution. It was revealed again that the tendency of SCC resistance was consistent with passivity.
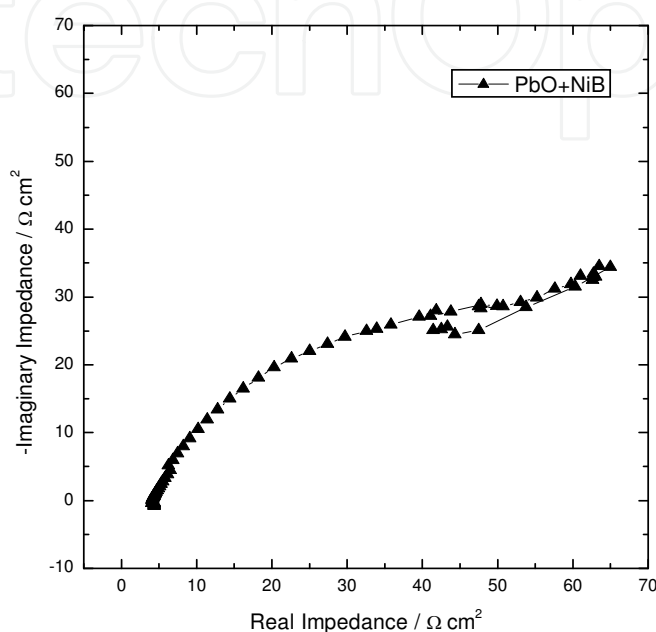

Fig. 13. Nyquist plot obtained from the electrochemical impedance measurements for the TT Alloy 600 immersed in the 0.1M NaOH solution with PbO + NiB at 315°C

From the results of SCC and oxide analysis, it was suggested that a lead incorporation in a surface oxide degrades an oxide passivity, which is related to a SCC susceptibility. By adding NiB into a solution, less incorporation of lead in an oxide retards the oxide degradation significantly leading to an improvement of its SCC resistance.

In Fig. 14, wetting angle obtained for the surface of Alloy 600 as a function of the solution is shown. Wetting angle was decreased as PbO and PbO+NiB were added into a high purity water as a reference solution. According to equation (12), we can consider two limiting cases.

$$\gamma_{SL} + \gamma_{LV} \cos\theta = \gamma_{SV} \qquad (12)$$

where γ_{SL}, γ_{LV}, γ_{SV} and θ represent the surface energy between a solid(Alloy 600) and a liquid(solution), the surface energy between a liquid and a vapor(air), the surface energy between a solid and a vapor and the wetting angle of a droplet between a solid/liquid and a liquid/vapor, respectively.

First, in the case of a complete wetting, the wetting angle is zero and $\gamma_{SL} + \gamma_{LV} = \gamma_{SV}$, which means that γ_{SV} is so large that a droplet is completely wetted. Second, in the case of a zero wetting, the wetting angle is 180° and $\gamma_{SV} + \gamma_{LV} = \gamma_{SL}$, which means that γ_{SL} is so large that a droplet is not wetted at all. In reference to the zero wetting case, it is expected that a

decrease of the wetting angle indicates a decrease of the surface energy between a solid and a liquid when γ_{LV} and γ_{SV} are not changed significantly by adding additive into a solution. From the result of Fig. 14, PbO is preferentially adsorbed on the Alloy 600 surface when PbO is added into an aqueous solution leading to a lead incorporation in a surface oxide. However, the wetting angle was decreased more when PbO and NiB were added into a solution simultaneously. This indicates that the NiB introduced into a solution competes with the PbO to adsorb on the surface of Alloy 600 and is more preferentially adsorbed on it leading to a lesser incorporation of lead in the oxide as shown in Figs. 11 and 12. As shown in Figs. 1 and 2, the thickness of the oxide layer whose composition was similar to the chemical composition of oxide layer formed in a solution without NiB was increased by the addition of NiB without PbO. Moreover the addition of NiB into a solution without PbO did not reveal any detrimental effect on the SCC resistance (Yi et al., 2005). Therefore, a fast adsorption of NiB on the Alloy 600 surface at an early stage of an exposure in an aqueous solution can affect an oxide properties and hence its SCC resistance. Inhibitive mechanism of NiB should be clarified more in the future.
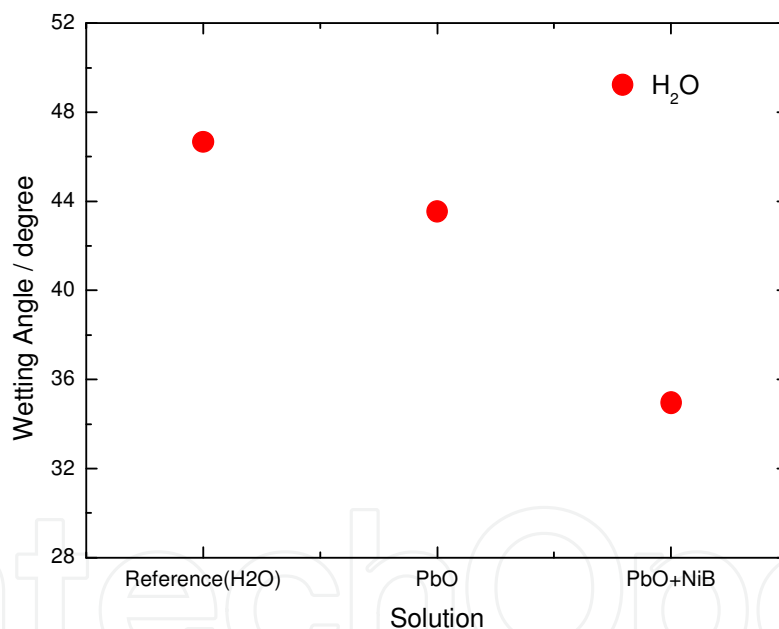

Fig. 14. Wetting angle obtained for Alloy 600 at 315ºC as a function of an ammonia solution: (a) without additive (reference solution), (b) with PbO and (c) with PbO and NiB (Kim, D.-J. et al., 2010).

4. Conclusions

The results are summarized as follows.
1. In the unleaded mild caustic solution, a relatively passive duplex oxide layer, i.e., porous nickel-rich outer layer (NiO and Ni(OH)$_2$) and dense chromium-rich inner layer (Cr$_2$O$_3$) was formed while the duplex oxide layer was not observed and cations were

depleted by lead incorporation in the oxide layer formed in the leaded mild caustic solution.

2. Lead was incorporated into the oxide layer as a metallic state and a lead oxide state. Lead incorporation into the oxide degraded the oxide passivity leading to the SCC susceptibility.

3. From the thermodynamic considerations supplemented by the experimental results in the high temperature leaded solution, the Ni as a Ni oxide state as well as the Ni as a metallic state can be depleted unlike Cr and Fe. Moreover cations in the oxide can be depleted by the Pb electrodeposition. The Pb incorporation would prevent the passive oxide formation composed of Ni, Cr, Fe and O.

4. HTMA Alloy 600 was susceptible to a PbSCC in a mild alkaline solution rather than a strong alkaline solution, whereas Alloy 690 was very susceptible to a SCC as well as PbSCC in highly caustic solution.

5. PbSCC was significantly reduced by adding NiB as an inhibitor, which was consistent with the reduction in an incorporated Pb amount and the increase of electrochemical impedance, accompanied with a significant recovery of the cation depletion. The passivity of the surface oxide was increased in the order of the surface oxide formed in a solution with PbO, PbO+NiB and a reference solution, which was in good agreement with the order of the SCC resistance. It is anticipated that the fast adsorption of NiB on the Alloy 600 surface at an early stage of an exposure in an aqueous solution can affect an oxide properties and hence its SCC resistance.

5. Acknowledgement

6. References

Castano-Marin, M. L.; Gomez-Briceno & D. and Hernandez-Arroyo, F. (1993). *Proc. of 6th Int. Symp. on Environmental Degradation of Materials in Nuclear Power Systems-Water Reactors*, p. 189, San Diego, CA, Aug. 1-5,.

Fruzzetti, K. (2005). *Workshop of Effects of Pb and S on the Performance of Secondary Side Tubing of Steam Generators in PWRs*, ANL, IL, May 24-27.

HSC Chemistry Database, 6.0.

Http://www.lasurface.com.

Hwang, S. S.; Kim, H. P. & Lim, Y. S. & Kim, J. S. & Thomas, L. (2007). *Corrosion Science*, Vol. 49, 3797.

Joint Committee on Power Diffraction Standards (JCPDS) - International Centre for Diffraction Data (ICDD) CD 2001(Card No. 47-1049).

Joint Committee on Power Diffraction Standards (JCPDS) - International Centre for Diffraction Data (ICDD) CD 2001(Card No. 74-0326).

Kim, D.-J.; Kim, H. P. (2009). *Proc. of 6th CNS Int. Steam Generator Conference*, p. 32, Toronto, Ontario, Nov. 8-11.

Kim, D.-J.; Kim, H. P. & Hwang, S. S. & Kim, J. S. & Park, J. (2010). *Met. Mater. Int.*, Vol. 16, 259.

Kim, D.-J.; Kwon, H. C. & Kim, H. P. (2008). *Corrosion Science*, Vol. 50, 1221.

Kim, D.-J.; Lim, Y. S. & Kwon, H. C. & Hwang, S. S. & Kim, H. P. (2010). *J. of Nanoscience and Nanotechnology*, Vol. 10, 85.

Kim, U. C.; Kim, K. M. & Lee, E. H. (2005). *J. Nuclear Materials*, Vol. 341, 169.

Lu, B.; Luo, J. & Lu, Y. (2008). *Workshop on Detection, Avoidance, Mechanisms, Modeling, and Prediction of SCC Initiation in Water-Cooled Nuclear Reactor Plants*, Beaune, Burgundy, France, Sept. 7-12.

Machet, A.; Galtayreis, A. & Zanna, S. & Klein, L. & Maurice, V. & Jolivet, P. & Foucault, M. & Combrade, P. & Scott, P. & Marcus, P. (2004). *Electrochim. Acta*, Vol. 49, 3957.

McIntyre, N. S.; Zetaruk, D. G. & Owen, D. (1979). *J. Electrochem. Soc.*, Vol. 126, 750.

MULTEQ calculation performed at ANL (2008).

Pourbaix, M. (1966). *Atlas of Electrochemical Equilibria in Aqueous Solutions*, Pergamon press Ltd.

Rincón, M. E.; Trujillo-Camacho, M. E. & Miranda-Hernández, M. & Cuentas-Gallegos, A. K. & Orozco, G. (2007). *J. Nanoscience and Nanotechnology*, Vol. 7, 1596.

Robertson, J. (1989). *Corrosion Science*, Vol. 29, 1275.

Sarver, J. M. (1987). *EPRI Workshop on Intergranular Corrosion and Primary Water Stress Corrosion Cracking Mechanisms*, p. C11/1, NP-5971, EPRI, Palo Alto.

Staehle, R. W. (2003). *Proc. of 11th Int. Symp. on Environmental Degradation of Materials in Nuclear Power Systems-Water Reactors*, p. 381, Stevenson, WA, Aug. 10-14.

Vaillant, F.; Buisine, D. & Prieux, B. & Gomez Briceno, D. & Castano, L. (1996). *Eurocorr 96*, p. 13/1, Nice.

Wright, M. D. & Mirzai, M. (1999). *Proc. of 9th Int. Symp. on Environmental Degradation of Materials in Nuclear Power Systems-Water Reactors*, p. 657, Newport Beach, CA, Aug. 1-5.

Yi, Y.; Eom, S. & Kim, H. & Kim, J. (2005). *J. Nucl. Mater.*, Vol. 347, 151.
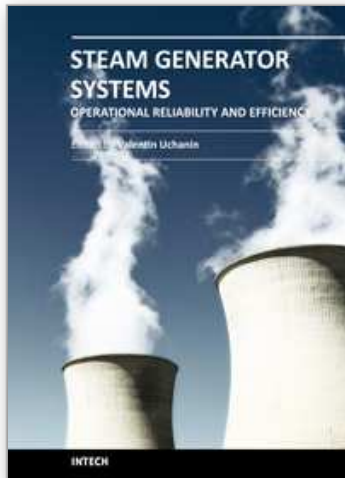
Steam Generator Systems: Operational Reliability and Efficiency

Edited by Dr. Valentin Uchanin

ISBN 978-953-307-303-3

Hard cover, 424 pages

Publisher InTech

Published online 16, March, 2011

Published in print edition March, 2011

The book is intended for practical engineers, researchers, students and other people dealing with the reviewed problems. We hope that the presented book will be beneficial to all readers and initiate further inquiry and development with aspiration for better future. The authors from different countries all over the world (Germany, France, Italy, Japan, Slovenia, Indonesia, Belgium, Romania, Lithuania, Russia, Spain, Sweden, Korea and Ukraine) prepared chapters for this book. Such a broad geography indicates a high significance of considered subjects.

How to reference

In order to correctly reference this scholarly work, feel free to copy and paste the following:

Dong-Jin Kim, Seong Sik Hwang, Joung Soo Kim, Yun Soo Lim, Sung Woo Kim and Hong Pyo Kim (2011). Analysis of Oxide on Steam Generator Tubing Material in High Temperature Alkaline Leaded Solution, Steam Generator Systems: Operational Reliability and Efficiency, Dr. Valentin Uchanin (Ed.), ISBN: 978-953-307-303-3, InTech, Available from: http://www.intechopen.com/books/steam-generator-systems-operational-reliability-and-efficiency/analysis-of-oxide-on-steam-generator-tubing-material-in-high-temperature-alkaline-leaded-solution

INTECH
open science | open minds